water

MDPI

Article

Transport of Cu^{2+} in Unsaturated Porous Medium with Humic Acid/Iron Oxide Nanoparticle (Fe_3O_4) Amendment

Shanshan Lin [1], Mengdi Shi [1], Qi Wang [1], Junlin Yang [1], Gubin Zhang [2], Xiangru Liu [1] and Wei Fan [1,*]

[1] School of Environment, Northeast Normal University, No. 2555, Jingyue Street, Changchun 130117, China; linss071@nenu.edu.cn (S.L.); shimd093@163.com (M.S.); WQ17833111126@163.com (Q.W.); yangjl950701@163.com (J.Y.); liuxr881@nenu.edu.cn (X.L.)

[2] Henan Key Laboratory of Groundwater Pollution Prevention and Rehabilitation, Zhengzhou 450001, China; zgubin2008@126.com

* Correspondence: fanw100@nenu.edu.cn

Abstract: Humic acid (HA) and iron oxide (such as Fe_3O_4) nanoparticles are widely distributed in soil, and their complex embedded in soil might affect the transport and fate of Cu^{2+} in the vadose zone, while Cu^{2+} is a serious threat to the underlying groundwater. In this study, we synthesized a composite of Fe_3O_4 nanoparticles coated with HA (HA@NPs) using as an amendment a packed sand matrix in the transport column experiments. The impacts of HA content and ion strength (IS) on Cu^{2+} transport in the unsaturated columns were investigated. The results showed that HA exhibited a stronger inhibition effect on Cu^{2+} transport, and a higher IS enhanced the mobility of Cu^{2+} in an unsaturated porous medium in the presence of HA@NPs. The recovery ratio (R_r) of Cu^{2+} breakthrough in the column decreased from 66.56% to 3.94% while the mass concentration ratio C_{HA}/C_{NPs} increased from 0 to 50 in the HA@NPs complex. The R_r increased by 1.64 times while the IS increased from 0 to 100 mM. Batch adsorption experiments, kinetics and isotherm models, and Fourier transform infrared (FTIR) spectra analysis were implemented to elucidate the underlying mechanism. It was found that HA embedded in the sand matrix could bind Cu^{2+} by forming stable chelate, while the IS-dependent Cu^{2+} transport could be attributed to the competitive adsorption between Na^+ and Cu^{2+}. Our study demonstrates that the physicochemical environment, as well as the presence of iron oxide nanoparticles and natural organic matter, can significantly impact Cu^{2+} transport in unsaturated porous medium.

Keywords: unsaturated porous media; Fe_3O_4 nanoparticles; humic acid; ionic strength; Cu^{2+} transport

Citation: Lin, S.; Shi, M.; Wang, Q.; Yang, J.; Zhang, G.; Liu, X.; Fan, W. Transport of Cu^{2+} in Unsaturated Porous Medium with Humic Acid/Iron Oxide Nanoparticle (Fe_3O_4) Amendment. *Water* **2021**, *13*, 200. https://doi.org/10.3390/w13020200

Received: 16 December 2020
Accepted: 13 January 2021
Published: 15 January 2021

1. Introduction

Copper (Cu) pollution poses a dangerous threat to the environment. In particular, China has the most widespread copper soil pollution problem [1,2]. According to the China Soil Pollution Survey in 2014, 2.1% of the contaminated sites in tests had soil polluted by copper [3]. Ionic copper (Cu^{2+}), namely the soluble state of copper, is one of the key soil pollutants that must be removed because of its biotoxicity and mobility [4]. Copper-bearing wastewater from smelting plants, chemical mechanical planarization, and mine drainage could break through the vadose zone and infiltrate into groundwater. This can pose serious risk to the environment and human health, as groundwater supply accounts for 17.5% of the total water supply in China [5]. Understanding the factors affecting transport and fate of Cu^{2+} in unsaturated porous media is thus essential. In particular, while humic acid (HA) and iron oxide (such as Fe_3O_4) particles are widely distributed in the soil, there have been few studies that examine how the embedded Fe_3O_4 particles and HA affect Cu^{2+} transport in unsaturated porous medium [6,7].

HA is the main organic component in the soil [8], and represents approximately 60% of soil organics [9]. A large number of branched hydrophilic and hydrophobic moieties,

as well as functional groups (i.e., carboxy, carbonyl, and hydroxyl), are linked to each other by the backbone of the aliphatic or aromatic units in HA [10]. This complex chemical structure determines the sensitivity and the physicochemical properties of HA to any given environmental factors [11]. HA becomes a repository for many pollutants due to its strong surface adsorption caused by the complexation and chelation between the functional groups of HA and the environmental pollutants [12]. The interactions between HA and heavy metals are mainly chemical complexation, cationic proton exchange, electrostatic adsorption, and flocculation [8,13]. The number of oxygen functional groups on the surface of the HA particles is a crucial factor that determines the nature of its interaction with heavy metals [14,15]. Hydrophilic and hydrophobic organics usually enhanced the mobility of heavy metals in clean sand, since the adsorption of heavy metals on the sand surface was inhibited after they were coated by these organics. The mediated transport depended on the inherent mobility of the organics in sand, and usually followed the order of hydrophilic matters > hydrophobic matters [16]. However, if the dissolved organic matter (DOM) was injected continuously, then ternay complexes (metals–DOM–sand medium) might form and substantially inhibit the mobility of heavy metals [17]. Ionic strength (IS) is recognized to compress the double electric layer and consequently influence the electro kinetic characteristics of macromolecular substance [18]. Thus, the reaction between HA and Cu^{2+} may be significantly affected by IS. The impacts of IS on the transport of mobile HA and colloid/nanoparticles (NPs) through porous medium have been reported [19]. Because of increased charge screening and charge neutralization effects, the increase of IS can weaken electrostatic repulsion between suspended NPs and between NPs and the medium particles, typically resulting in NPs aggregation and strong deposition at porous medium surfaces [18,19]. However, the role of IS in the transport of Cu^{2+} in porous medium with embedded HA/ Fe_3O_4 NPs is not well understood.

Moreover, it is important to understand the transportation and interaction between NPs and heavy metals in unsaturated porous medium because the vadose zone represents both the medium that is polluted with Cu^{2+} and the natural barrier that prevents Cu^{2+} from being transported into groundwater [20]. According to survey work done by Corapciogl et al. (1999) [21], there is an average of 10^8–10^{17} colloidal particles (biocolloids, inorganic colloids, and organic colloids) per liter in the groundwater. This indicates that colloids/NPs can carry pollutants such as heavy metals into the groundwater [22]. Most studies focus on the transportation of colloids in a saturated porous medium, where the colloids are adsorbed across the solid-water interface (SWI) and deposited in the medium through multi-particle bridging and the physical interception of steric hindrance [23,24]. Bradford et al. showed that the colloid adsorption across an air-water interfaces (AWI) in an unsaturated porous medium is both strong and irreversible because of the negative charge of the gas–liquid interface [25,26]. Processes such as the deposition and transportation of colloids and heavy metals are controlled by the chemical and hydrodynamic conditions of the porous medium, such as ionic strength, pH, moisture content, and flow rate [26,27]. Few studies have examined the heavy metal transport in an unsaturated porous medium embedded with NPs coated with organic material. In particular, Fe_3O_4 NPs usually appear in soil accompanied by Cu^{2+} in mining areas [28,29], or magnetic Fe_3O_4 NPs are often added artificially for soil remediation because they can be easily separated from the soil matrix through an external magnet to avoid secondary pollution [30,31].

The objective of this work was thus to examine the influence of the presence of HA-coated Fe_3O_4 NPs (HA@NPs) embedded in porous medium and solution IS on Cu^{2+} transport through the vadose zone. The approach focused on a systematic identification of the mechanism that mediated Cu^{2+} transport in unsaturated porous medium with HA@NPs amendment. The Cu^{2+} transport column experiment results were interpreted through monitoring of breakthrough curves (BTCs), a batch adsorption experiment, and surface property measurements of targeted compounds.

2. Materials and Methods

2.1. Porous Media

For the porous medium in our experiments, we collected natural river sand (sifted through 1 mm sieve) from the Yitong River in Changchun, China. Sands with an average diameter of 0.53 mm represent the medium in the vadose zone overlying the local aquifer. The sand was air dried and washed with deionized (DI) water five times to remove impurities. The sand was then immersed in 4% HCl for 24 h, rinsed with deionized water, soaked in a 1 M NaOH solution for another 24 h, and finally washed repeatedly with deionized water until the filtrate had a pH of 5.5 [32,33]. The pH 5.5 used herein aimed to avoid precipitation of Cu. The sand was then dried at 105 °C overnight.

2.2. Preparation of Humic Acid (HA)-Coated Iron Oxide (Fe_3O_4) Nanoparticles (NPs)

The Fe_3O_4 NPs were purchased from the Shanghai Macklin Biochemical Technology Co., Ltd., China with a diameter of 20 nm (purity $\geq$ 99.5%). We added 3.4 g of the NPs to 1.0 L of ultra-pure water, mixed the solution in a sonicator bath for 6 h, and finally deflocculated the solution by heating it at 70 °C with sufficient stirring until the slurry changed to be a stable suspension. In order to avoid the particle aggregation, the NPs were ultrasonicated for 3 h (Fuyang F-060S, 450 W, 40 KHz) again prior to being coated with HA, the average size of NPs was 584 nm measured by ZetaSizer Nano ZS (Malvern Instruments, Worcestershire, UK) (Figure S1 in Supplementary Material). The stock suspension was stored at 4 °C.

We dissolved 1.7 g of HA (acquired from the Tianjin Guangfu Fine Chemical Research Institute, Tianjin, China) in 100 mL of 1 M NaOH under constant stirring at 25°C until the HA had dissolved into the solution. We then introduced ultrapure water to create a final solution with mass concentration ratio C_{HA}/C_{NPs} values of 10, 20, 30, and 50. Every mixture of HA and Fe_3O_4 NPs was stirred for 50 h; we obtained HA@NPs by injecting that mixture with 0.01 M HCl and 0.01 M NaOH until the pH reached a value of 5.5. The suspension of HA@NPs was then mixed with the cleaned sand at 25 °C until the HA@NPs fully coated the surface of the sand particles.

2.3. Characterization of HA, Fe_3O_4 NPs, and HA-Coated Fe_3O_4 NPs

Fourier transform infrared (FTIR) spectra of sand, HA, Fe_3O_4 NPs, and HA@NPs were recorded in the range of 600–4000 cm^{-1} using a 330 FTIR microscope (Thermo Fisher Scientific, Waltham, MA USA) [33]. The zeta potential (ZP) and hydrodynamic diameter of the aforementioned four mediums was measured using ZetaSizer Nano ZS (Malvern Instruments, Worcestershire, UK) [34]. We measured the magnetic properties of the Fe_3O_4 NPs and HA@NPs using a vibrating sample magnetometer (Magnetic Property Measurement System XL-7, Quantum Design, San Diego, CA USA) following the process described by Ghosh et al. (2011) [35].

2.4. Column Transport Experiments

Transport experiments were conducted by pumping Cu^{2+} solution (50 mg L^{-1}) through an acrylic column packed with a sand matrix (Figure 1). The acrylic column was 8 cm in diameter and 50 cm in height; porous circular plates were installed at the top and bottom of the column to prevent particles from escaping. The column was packed with 3.4 kg of granular media with a density of 1.36 g/cm^3. The porosity of the packed medium was 0.378 on average, and the hydraulic dispersion coefficient was estimated to be 0.178 cm^2 min^{-1}. Two peristaltic pumps at the inlet and outlet of the column were used to regulate the moisture content and to control the downward flow rate. The target moisture content (80% water saturation) was obtained according to the method developed by Esfandyari Bayat et al. 2015 [36]. The tensiometers (Meter T5x, München, Germany) at both ends read the same values, indicating uniform flow conditions.

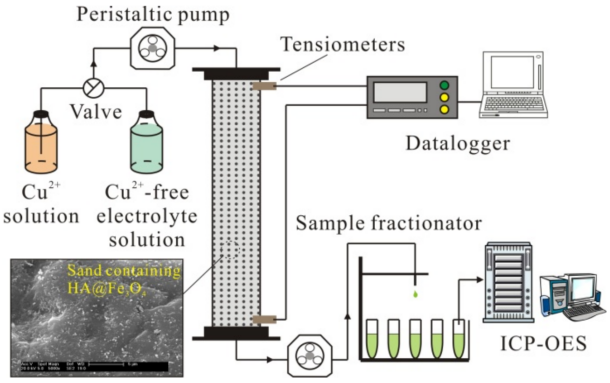

Figure 1. Schematic of the experimental set-up.

There are two groups of column experiment in this study. (1) Group one was performed to examine the impact of the presence of HA coated Fe_3O_4 NPs (HA@NPs) embedded in porous medium on Cu^{2+} transport. Six types of packed medium in the columns were sand only (sand), sand containing Fe_3O_4 NPs (NPs + sand), 1HA@NPs + sand, 2HA@NPs + sand, 3HA@NPs + sand, and 5HA@NPs + sand, wherein the coefficients of HA, I = 1, 2, 3, and 5, mean i g HA embedded in 1 kg sand. The content of Fe_3O_4 NPs in the sand was 0.1 g kg^{-1}. Accordingly, the C_{HA}/C_{NPs} was raised from 0 to 10, 20, 30, and 50, respectively. The solution IS was 5 mM and pH = 5.5. (2) In group two, three types of packed medium were used: sand, NPs + sand, and 1HA@NPs + sand. The Cu^{2+} breakthrough curves under IS 0, 5, 10, 50, 100 mM were investigated in each medium to indicate the role of IS. The solution pH was 5.5.

For each column experiment, 10 pore volumes (PVs) of the background electrolyte solution of interest were first passed through the column to ensure that the column was fully equilibrated with this solution. This process also aimed to remove all possible remobile particles in the fixed-bed matrix in the column, and the spatial distribution of embedded particles in the column was determined immediately after this elution process. The mechanism for the stability of the packed medium was elucidated by Derjaguin–Landau–Verwey–Overbeek (DLVO) interaction energy calculations [33].

Then, suspension of Cu^{2+} within the same background electrolyte composition was injected into the packed column for 16.5 PVs (phase 1), followed by elution with Cu^{2+}-free solution again (phase 2). The outflow from the columns was connected by an auto fraction sampler (Huxi CBS-A 100, Shanghai, China), and the effluent Cu^{2+} concentration was monitored using an inductively coupled plasma optical emission spectrometer (ICP-OES, Avio 200, PerkinElmer, Waltham, MA, USA). The effluent mass recovery rate (R_r) was calculated by integrating the BTCs.

2.5. Batch Adsorption–Desorption Experiments

Both batch adsorption and desorption experiments were carried out to explain the Cu^{2+} transport behaviors in different packed mediums and under different IS. In the adsorption experiments, three types of medium, sand, NPs + sand, and 1HA@NPs + sand were used as adsorbents. We measured the Cu^{2+} sorption kinetics by mixing 20 g of targeted adsorbent with 100 mL of Cu^{2+} solution (50 mg/L) with a pH of 5.5 and IS of 0, 5, 10, 50, and 100 mM in Teflon centrifuge tubes. The time required for equilibrium was set as 5 h following a previous kinetic study [37], and the differences of the concentration values of Cu^{2+} were actually less than 1% after 3 h indicating the feasibility of 5 h. The adsorption dynamics of Cu^{2+} in each adsorption system was obtained by measuring Cu^{2+} concentration at time interval of 5–60 min. The tubes at specific sampling time were centrifuged for 30 min at 12,000 rpm, and the supernatant was filtered by a 0.45-μm membrane, followed by Cu^{2+} measurement by ICP-OES. The Cu^{2+} desorption kinetics were then measured by mixing the Cu^{2+}-rich porous medium with 100 mL of a 0.01 M NaCl solution and shaking the solution at room temperature (23–25 °C) for 5 h. The Cu^{2+} concentrations of the solutions

were determined at the same time interval as the aforementioned adsorption experiment. The mechanisms underlying the adsorption process were further investigated using the pseudo-1st order and pseudo-2nd order rate equations to fit the adsorption experimental data as described by Chen et al. [38]. The adsorption equilibrium data were fitted using the Langmuir and Freundlich isotherms to provide quantitative information for adsorption isotherms, respectively [39].

3. Results and Discussion

3.1. Surface Properties of HA, Fe_3O_4 NPs, HA@NPs, and Sand

FTIR spectra were used to identify the surface functional groups for the HA, Fe_3O_4 NPs, 1HA@NPs, and sand (Figure 2a). For sand, the main peaks around 998 and 773 cm^{-1} are attributed to symmetric Si-O-Si vibrations [40]. The FTIR spectrum of HA reveals a broad band at 3255 cm^{-1}, attributed to O–H and trace N–H stretching [41]. The peak at 1565 cm^{-1} and 1378 cm^{-1} are identified as N–H bending vibration and C–N stretching vibrations while peaks around wavelengths 1007 cm^{-1} and 912 cm^{-1} correspond to C–H stretching [42]. The band located at 1039 cm^{-1} in the FTIR spectrum of Fe_3O_4 NPs indicates the symmetric stretching vibration of the Fe–O stretching. While the NPs are coated by HA, the main peak is assigned to C–H stretching. Both the surface hydroxyls (Si–OH) on sand and (3623 cm^{-1}) abundant –OH on HA can provide adsorption sites for Cu^{2+}.

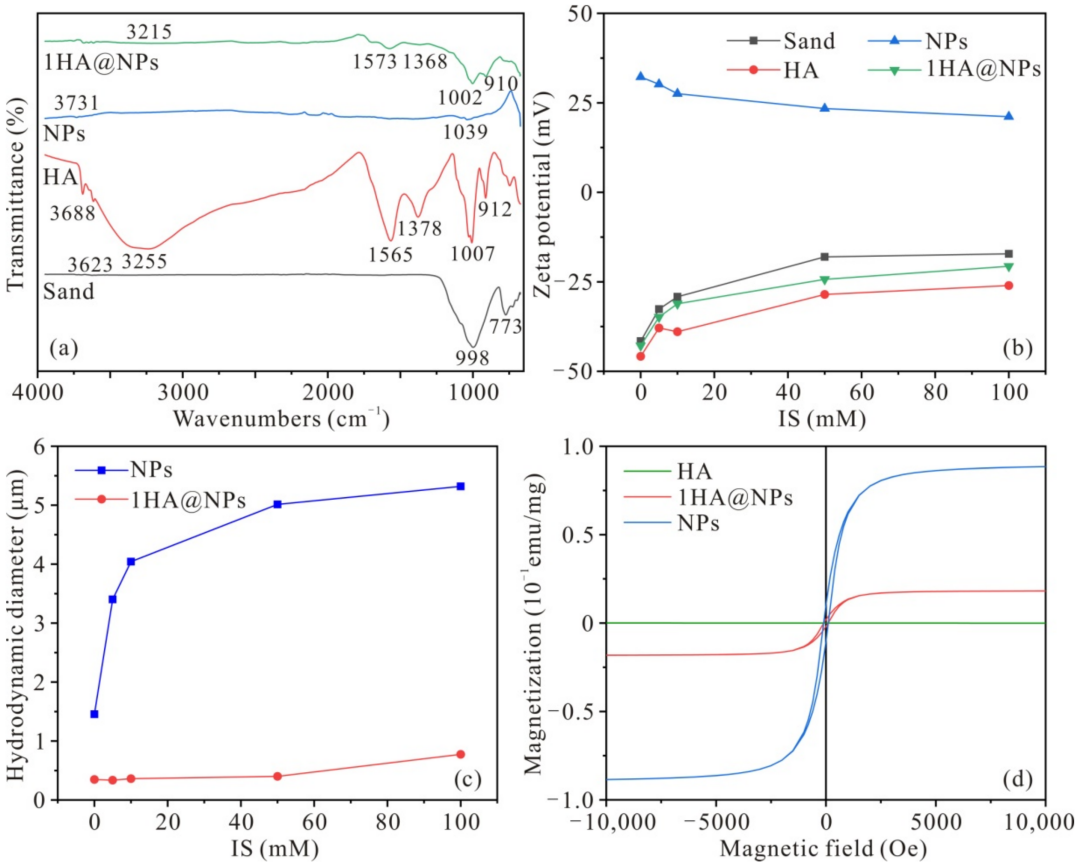

Figure 2. (**a**) Fourier transform infrared (FTIR) spectra of humic acid (HA), iron oxide (Fe_3O_4) nanoparticles (NPs), 1HA@NPs, and sand. (**b**) Influence of IS on the zeta potential of HA, Fe_3O_4 NPs, 1HA@NPs, and sand. (**c**) Influence of ion strength (IS) on the hydrodynamic diameter of Fe_3O_4 NPs and 1HA@NPs. (**d**) The hysteresis loops of HA, Fe_3O_4 NPs and 1HA@NPs.

Figure 2b,c shows the zeta potentials and hydrodynamic diameters of different samples when IS varied from 0 to 100 mM. The electrokinetic measurements showed that the HA, 1HA@NPs and sand were negatively (approximately –25 mV) charged over the range of solution conditions investigated, and the Fe_3O_4 NPs is positively charged (approximately 25 mV). This indicates considerable electrostatic attractive forces between Cu^{2+} and these compounds. The particles size increased obviously with IS, while the zeta potentials became less negative. Increasing the IS results in compression of diffuse double layers around charged surfaces, thus reducing the repulsive forces between the particles and decreasing their stability to form aggregates [32]. By contrast, the HA coating increased the stability of Fe_3O_4 NPs (Figure 2c). As shown in Figure 2d, the hysteresis loops of Fe_3O_4 NPs and 1HA@NPs are standard S-shaped curves without remanence, indicating that the coated HA did not destroy the intrinsic superparamagnetism. Adding the HA coating to the NPs decreased the saturation magnetization value because HA has diamagnetic resistance, and a magnetically dead layer was formed with oxygen and other elements on the surface of the NPs [35]. Some studies demonstrated that the magnetic properties of NPs were attenuated through interaction with the HA surface groups [43–45], our magnetic coercivity values for NPs and 1HA@NPs are similar to those of previously published values [46]. Thus, HA reduced the magnetic force between the HA@NPs particles and improved their stability. Moreover, the decreased magnetization still could be observed after rinsing of the HA@NPs, it thus also proved the stability of the HA–NP complex.

3.2. Stability of HA-Fe_3O_4 NP-Sand Fixed-Bed in the Column

One important premise of the transport experiments is the stability of the fixed-bed matrix in the column. The breakthrough curves of Cu^{2+} should not be disrupted by the possible presence of mobile particles. Herein, we discuss the possible stabilization mechanisms for the HA-Fe_3O_4 NP-sand system. Calculated DLVO interaction energies (Φ) between sand and the NPs or 1HA@NPs are plotted as functions of separation distance in Figure 3, and the data are depicted in terms of kT, where k is the Boltzmann constant and T is Kelvin temperature. For NPs, as shown in Section 3.1, the positively charged surface made this scenario as a "favorable condition" for attachment on negative sand surface. NPs were readily deposited into the primary energy minimum ($\Phi_{primary\text{-}min}$) (Figure 3a). For 1HA@NPs, while the presence of the high Φ_{max} would prevent the deposition of particles into the primary energy minimum (Figure 3b), they could be immobilized within the secondary energy minimum ($\Phi_{second\text{-}min}$) [33]. Indeed, the calculated interaction energy profiles showed the presence of the $\Phi_{second\text{-}min}$ and the depth of the $\Phi_{second\text{-}min}$ increased with IS, which indicated that it became more likely for HA@NPs to be retained with sand in the column under high IS. The release of NPs and 1HA@NPs from the column during sequential elution experiment and retention profiles of the two particles after 10 PVs elution finished at IS = 0 mM are shown in Figure 3c,d. The release of immobilized particles could be negligible after 8 PVs elution (near 0 mg L^{-1}), and the distributions of particles along the column were uniform.

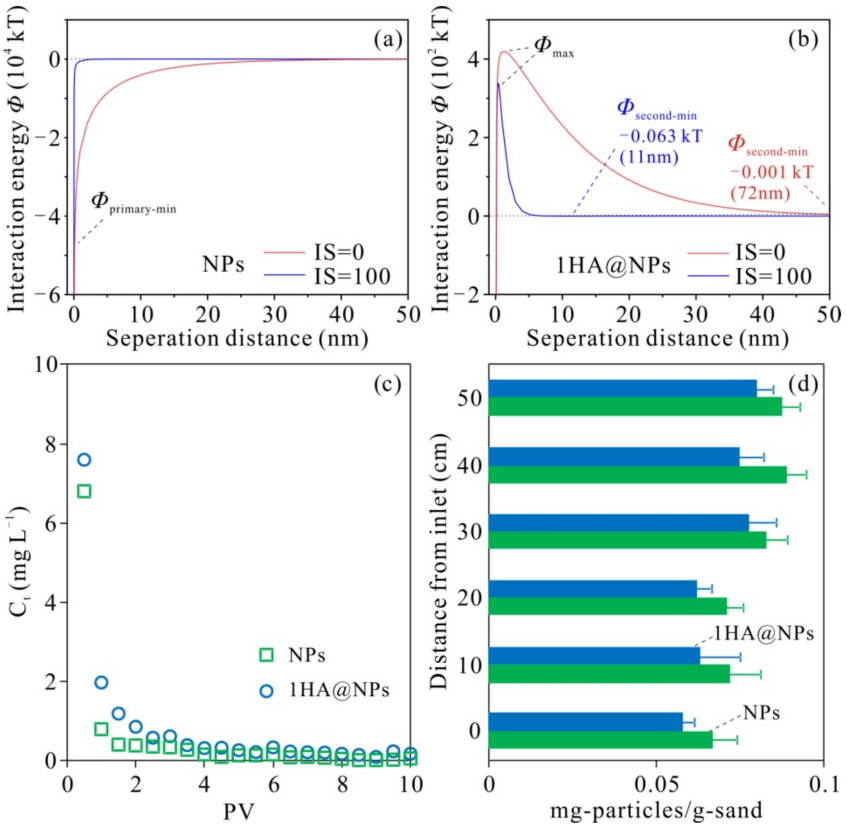

Figure 3. Calculated DLVO interaction energy plotted as a function of separation distance between the sand surface and NPs (**a**) or 1HA@NPs (**b**) surface at IS = 0 mM and 100 mM. Release of NPs and 1HA@NPs from the column during sequential elution experiment (**c**) and retention profiles of the two particles after 10 pore volumes (PVs) elution finished (**d**) (IS = 0 mM).

3.3. Effect of the HA-Coated Fe_3O_4 NPs Embedded in Sand Matrix on Cu^{2+} Transport

As shown in Figure 4, the normalized effluent Cu^{2+} concentration C/C_0 was plotted as a function of PV. The deposition of Cu^{2+} increased (C/C_0 decreased) with increasing HA content in all packed media (Figure 4a and Table 1). The maximum breakthrough concentrations, $(C/C_0)_{max}$, were decreased from 0.857 to 0.810, 0.647, 0.560, and 0.170 finally when C_{HA}/C_{NPs} was raised from 0 (NPs + sand) to 10 (1HA@NPs + sand), 20 (2HA@NPs + sand), 30 (3HA@NPs + sand), and 50 (5HA@NPs + sand), respectively. The corresponding R_r values were 66.56%, 47.40%, 33.72%, 19.21%, and 3.94%, respectively. As a control, the $(C/C_0)_{max}$ and R_r in pure sand were 0.859and 66.96%. These results indicate that HA impedes the transportation of Cu^{2+}.

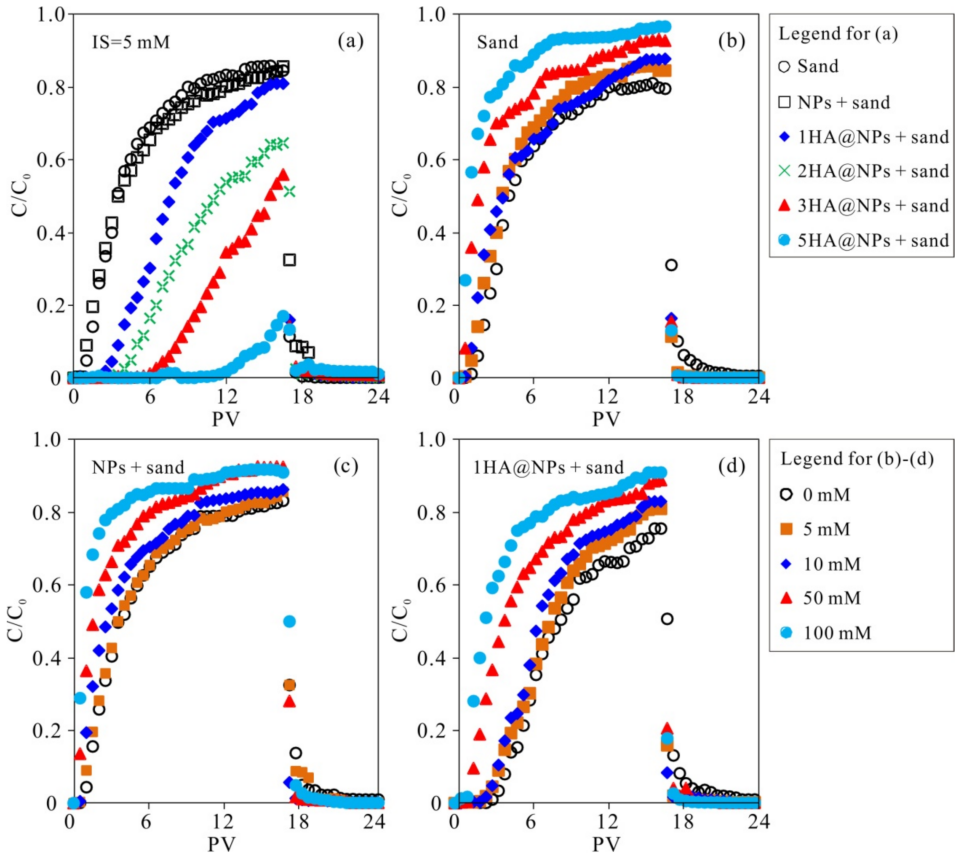

Figure 4. (**a**) Breakthrough curves of Cu^{2+} in columns packed with different medium, sand, NPs + sand, 1HA@NPs + sand, 2HA@NPs + sand, 3HA@NPs + sand, and 5HA@NPs + sand; the IS was 5 mM and pH = 5.5; (**b**), (**c**) Breakthrough curves of Cu^{2+} in columns packed with sand (**b**), NPs + sand (**c**), and 1HA@NPs + sand (**d**). The IS varied from 0 to 100 mM, while pH = 5.5.

Table 1. Quantifying the breakthrough curves of Cu^{2+} under different experimental conditions.

Medium	IS (mM)	pH	$(C/C_0)_{max}$	R_r
Sand	5	5.5	0.859	66.96%
NPs + sand	5	5.5	0.857	66.56%
HA@NPs + sand	5	5.5	0.810	47.40%
2HA@NPs + sand	5	5.5	0.647	33.72%
3HA@NPs + sand	5	5.5	0.560	19.21%
5HA@NPs + sand	5	5.5	0.170	3.94%
Sand	0	5.5	0.811	62.98%
	5	5.5	0.859	66.96%
	10	5.5	0.878	66.71%
	50	5.5	0.932	78.85%
	100	5.5	0.967	87.39%
NPs + sand	0	5.5	0.832	65.71%
	5	5.5	0.857	66.56%
	10	5.5	0.863	70.21%
	50	5.5	0.918	79.75%
	100	5.5	0.926	85.92%
HA@NPs + sand	0	5.5	0.756	44.83%
	5	5.5	0.810	47.40%
	10	5.5	0.830	50.70%
	50	5.5	0.889	65.12%
	100	5.5	0.910	73.53%

As shown in Equations (1) and (2), Cu^{2+} was first adsorbed on the surface of HA@NPs and sand by electrostatic attraction. Then, as shown in Equation (3), Cu^{2+} complexed with the functional groups (–COOH, –C=O) on the surface of HA@NPs and sand, which was controlled by proton exchange between Cu^{2+} and H^+ [34,47]. This HA@NPs that occurred in the potential layer of HA, is irreversible for Cu^{2+}. Additionally, some Cu^{2+} attached on HA@NPs to produce the stable chelate, and thus Cu^{2+} was immobilized by the HA@NPs.

$$Sur(H^+/Na^+)_m + Cu^{2+} \rightarrow Sur(H^+/Na^+)_{m\text{-}r} \ldots Cu^{2+} + r(H^+/Na^+), \quad (1)$$

$$Sur\text{-}O^- + Cu^{2+} \rightarrow Sur\text{-}O^- \ldots Cu^{2+}, \quad (2)$$

$$Sur\text{-}(O_nH_m)^{-n+m} + Cu^{2+} \rightarrow Sur\text{-}(O_nH_m\text{-}Cu)^{-n+m-r+2} + rH^+, \quad (3)$$

where "*Sur*" is the particle surface, "..." is an electrostatic action, and *n*, *m*, and *r* are constants. The Cu^{2+} ratio is stable in Equations (1)–(3) [48].

HA@NPs either adhered to the sand surface or accumulated in the porous medium AWI. According to Akbour et al. (2013) [10], the adsorption of HA on the surface of positively charged sand is primarily dependent on electrostatic interaction, and secondarily dependent on the interaction between the non-polar sites of the sand and the hydrophobic groups of the HA. Even if HA carried the same charge as the sand, HA could also be adsorbed onto the sand surface, and the amount of adsorption would surpass the amount of desorption because the HA function groups undergo ligand exchange with the sand [12,49]. The HA@NPs adhering to the sand might be caused by the similarity in the surface chemistries as HA. For the SWI and the AWI in the unsaturated porous medium, some studies indicate that the increased hydrodynamic diameter of HA@NPs could result in physical interception such as multi-particle bridging, steric hindrance, or surface deposition [23]. When the hydrodynamic diameters of the particles exceeded the AWI thickness, HA@NPs were more easily captured by the nearby AWI [26]. Additionally, the oscillating ring produced by water absorption between the particles hindered the migration of HA@NPs [50].

3.4. Effect of Ion Strength (IS) on Cu^{2+} Transport in Diverse Unsaturated Porous Media

Figure 4b–d shows the transport of Cu^{2+} in three types of porous medium with different IS values. The $(C/C_0)_{max}$ values of Cu^{2+} in each BTC and R_r are shown in Table 1. Taking the medium HA@NPs + sand as an example, when the value of IS increased from 0 to 5, 10, 50, and 100 mM, the $(C/C_0)_{max}$ values of Cu^{2+} increased from 0.756 to 0.810, 0.830, 0.889, and 0.910, respectively, while the corresponding R_r = 44.83%, 47.40%, 50.70%, 65.12%, and 73.53%, respectively. This IS-dependent Cu^{2+} transport can be attributed to the competitive adsorption between Na^+ and Cu^{2+}. As the IS of the solution increased, a large amount of Na^+ ions occupied the negatively charged adsorption sites on the surface of the sand and HA [51]. Those Na^+ ions neutralized the negative charges on the surface of the sand and HA, which reduced both the electrostatic force between the Cu^{2+} and the negative ions adsorbed at the electrical adsorption sites and the total number of Cu^{2+} ions on the surface of sand and HA. Based on the limit equation and the Bader–Shock theory, IS is negatively correlated with the activity coefficient of ions; the higher IS value corresponds to a lower initial activity of Cu^{2+} in the solution [52]. As a result, more Cu^{2+} were transported through the column.

3.5. Adsorption Characteristics of Cu^{2+} on Different Types of Media

Figure 5 depicts the time-dependent Cu^{2+} adsorption and desorption capacity of three media across varying IS (0, 5, 10, 50, and 100 mM), pure sand, NPs + sand, and 1HA@NPs + sand. In all adsorption media, the Cu^{2+} concentration in the liquid phase exhibited a rapid decrease within the initial 1–1.5 h which contributed to > 90% of the total adsorption, followed by a gradual decrease. Compared with the adsorption processes, the desorption of Cu^{2+} was relatively weak (<6 mg/L after 300 min). The aqueous Cu^{2+} concentration in

the desorption system was an order of magnitude lower than that in the adsorption system. This is in accord with the observation in transport experiments. The C/C_0 of Cu^{2+} quickly reached 0 after elution by 4–5 PVs Cu^{2+}-free solution (phase 2), suggesting that the release of pre-deposited Cu^{2+} could be negligible under the same IS.

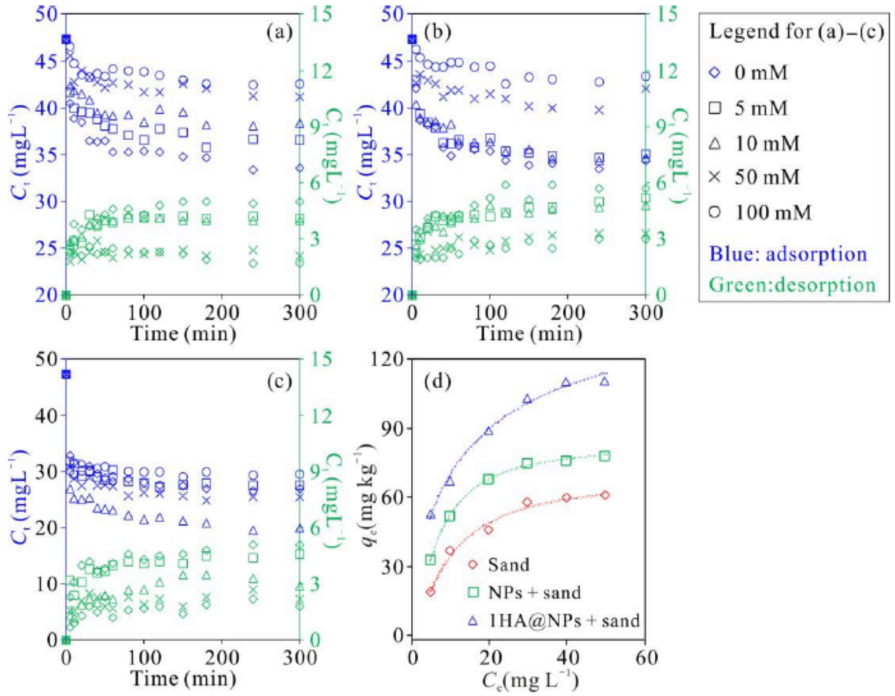

Figure 5. The adsorption and desorption of Cu^{2+} on (**a**) pure sand (**b**) NPs + sand (**c**) 1HA @NPs + sand at different IS values; (**d**) Adsorption isotherms of Cu^{2+} on the aforementioned mediums, and the dotted lines were the Langmuir isotherm fitting lines.

Table 2 and Figure 6a–c present the data fitting results of the pseudo-2nd-order kinetic model, which delineates that the entire adsorption process is generally controlled by chemisorption [39]. The results demonstrate the superior performance of the 2nd-order model with correlation coefficients $R^2 > 0.98$ and modeled q_e values closer to the measured results. The R^2 values of the pseudo-1st-order model were all less than 0.89 (data not shown here). This indicates the greater suitability of the pseudo-2nd-order model in describing the adsorption mechanism and consequently illustrates the predominance of chemical interactions thereof. The fitting results of the Cu^{2+} adsorption isotherm data indicated that the Langmuir model exhibited a stronger correlation (R^2 = 0.987–0.997) than the Freundlich model (Table 3 and Figure 6d). This suggests that the binding of Cu^{2+} on the porous medium in testing is a monolayer sorption.

The influences of IS and HA coating on Cu^{2+} adsorption thus supports the results of Cu^{2+} transport in the columns. The increasing HA concentration was linked with an enhancement in Cu^{2+} adsorption on the media, which was confirmed by the increase in k_2 and K_L (Table 3). Electrolytes inhibited Cu^{2+} adsorption and accelerated Cu^{2+} desorption on the surface of mediums. The scenario with higher IS displayed lower k_2, which thus led to more Cu^{2+} breakthrough in the column. This phenomenon could still be explained by either the competition for adsorption sites [53] or the competition for complexation sites on the outer-sphere surface between Na^+ and Cu^{2+} [54,55]. An X-ray energy dispersive spectrometer mapping graph was provided in Figure S2 to confirm the Cu adsorption.

Table 2. Fitted parameters of the adsorption kinetics models for the adsorption of Cu^{2+} in different media, with the IS of 0–100 mM.

Porous Medium	Parameters	IS (mM)				
		0	5	10	50	100
Sand	$q_{e,exp}$ (mg kg^{-1})	0.0698	0.0538	0.0458	0.0308	0.0243
	$q_{e,cal}$ (mg kg^{-1})	0.0706	0.0558	0.0464	0.0312	0.0255
	k_2 (min^{-1})	0.0018	0.0017	0.0016	0.0015	0.0011
	R^2	0.996	0.995	0.991	0.984	0.979
NPs + sand	$q_{e,exp}$ (mg kg^{-1})	0.0673	0.0643	0.0625	0.0323	0.0215
	$q_{e,cal}$ (mg kg^{-1})	0.0691	0.0666	0.0643	0.0394	0.0230
	k_2 (min^{-1})	0.0022	0.0021	0.0021	0.0020	0.0018
	R^2	0.997	0.998	0.996	0.986	0.955
1HA@NPs + sand	$q_{e,exp}$ (mg kg^{-1})	0.1380	0.1100	0.1030	0.0990	0.0895
	$q_{e,cal}$ (mg kg^{-1})	0.1390	0.1110	0.1000	0.1050	0.0895
	k_2 (min^{-1})	0.0028	0.0022	0.0021	0.0021	0.0018
	R^2	0.999	0.999	0.999	0.999	0.999

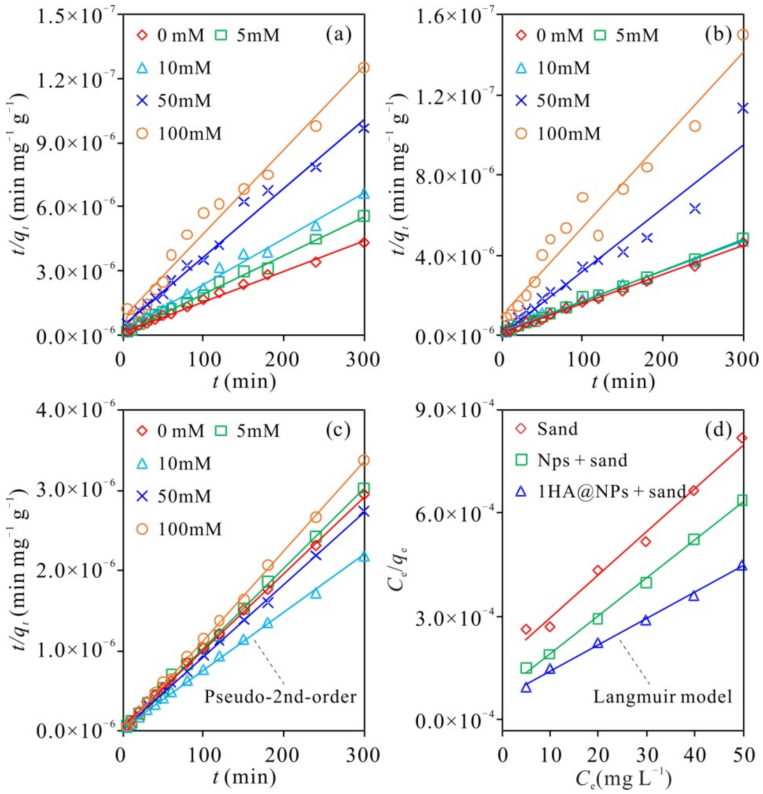

Figure 6. Pseudo-2nd order kinetic plot for Cu^{2+} adsorption processes on (**a**) pure sand, (**b**) NPs + sand, and (**c**) 1HA @NPs + sand at different IS values; (**d**) fitting results of Langmuir models for Cu^{2+} adsorption.

Table 3. Fitted parameters of the isotherm models for the adsorption of Cu^{2+} in different media, with an IS of 5 mM.

Models	Parameters	Porous Medium		
		Sand	NPs + Sand	1HA@NPs + Sand
Langmuir	q_m (mg kg^{-1})	79.365	90.909	130.208
	K_L (L mg^{-1})	0.075	0.121	0.133
	R^2	0.987	0.997	0.997
Freundlich	$1/n$	0.490	0.364	0.337
	K_F (L mg^{-1})	10.132	20.696	31.414
	R^2	0.924	0.922	0.985

4. Conclusions

In this study, we conducted laboratory experiments in order to investigate the transport of Cu^{2+} in unsaturated columns with humic acid/iron oxide NP (Fe_3O_4) amendment under different IS conditions. We found that the presence of HA stabilized Fe_3O_4 NPs in a sand matrix and was effective in restraining the transport of Cu^{2+}. The mobility of Cu^{2+} in the packed sand columns was enhanced at higher IS values. Complexation, electrostatic attractive force, hydration, oxygen-containing functional groups, surface attachment, and AWI attachment are all mechanisms or features that may be responsible for the retention and transport of Cu^{2+} in the unsaturated porous media embedded with HA@NPs. These conclusions were supported by the adsorption tests and modeling analyses. The presence of HA and NPs in the medium, and the IS change altered the fate, transport and diffusion risk of Cu^{2+} contamination during unsaturated seepage. Note that only monovalent electrolyte solution (NaCl) was used for IS modulation in the current study. We suggested that studies of the influences of cation composition in divalent solutions (Ca^{2+} or Mg^{2+}) or in mixed systems (Na-Ca-Mg) are necessary, because Na^+, Ca^{2+} and Mg^{2+} generally coexist in natural groundwater and their relative composition varies with hydro-geochemical process. In addition to Fe_3O_4 NPs, many natural organic/inorganic colloids and engineered nanomaterials are present in the soil environment, which also tend to associate with dissolved organic materials and heavy metals. Our findings thus provide a reference for delineating the ternary interactions and the consequences of these interactions, which will be an improved comprehension of the environmental risk of heavy metals in complex systems containing organic materials and colloids/NPs.

Supplementary Materials: The following are available online at https://www.mdpi.com/2073-4441/13/2/200/s1, Figure S1: Size distribution of Fe_3O_4 nanoparticles, Figure S2: X-ray energy dispersive spectrometer mapping to confirm Cu adsorption.

Author Contributions: Conceptualization, S.L. and G.Z.; Data curation, M.S.; Formal analysis, M.S.; Funding acquisition, S.L. and W.F.; Investigation, M.S., Q.W. and J.Y.; Methodology, M.S.; Project administration, S.L. and W.F.; Resources, S.L.; Software, X.L.; Supervision, W.F.; Validation, Q.W. and J.Y.; Visualization, W.F.; Writing—original draft, S.L. and W.F.; Writing—review and editing, S.L., X.L. and W.F. All authors have read and agreed to the published version of the manuscript.

Funding: This work was supported by the National Natural Science Foundation of China [NSFC No. 41772236 and 51978135]; and the Science and Technology Department of Changchun City [17SS027].

Institutional Review Board Statement: Not applicable.

Informed Consent Statement: Not applicable.

Data Availability Statement: The data presented in this study is contained within the article and supplementary materials.

Conflicts of Interest: The authors declare no conflict of interest.

References

1. Duan, Q.; Lee, J.; Liu, Y.; Chen, H.; Hu, H. Distribution of Heavy Metal Pollution in Surface Soil Samples in China: A Graphical Review. *Bull. Environ. Contam. Toxicol.* **2016**, *97*, 303–309. [CrossRef]
2. Yang, Q.; Li, Z.; Lu, X.; Duan, Q.; Huang, L.; Bi, J. A review of soil heavy metal pollution from industrial and agricultural regions in China: Pollution and risk assessment. *Sci. Total Environ.* **2018**, *642*, 690–700. [CrossRef]
3. Li, T.; Liu, Y.; Lin, S.; Liu, Y.; Xie, Y. Soil Pollution Management in China: A Brief Introduction. *Sustainability* **2019**, *11*, 556. [CrossRef]
4. Mackie, K.A.; Mueller, T.; Kandeler, E. Remediation of copper in vineyards-A mini review. *Environ. Pollut.* **2012**, *167*, 16–26. [CrossRef] [PubMed]
5. Wang, Y.; Zheng, C.; Ma, R. Review: Safe and sustainable groundwater supply in China. *Hydrogeol. J.* **2018**, *26*, 1301–1324. [CrossRef]
6. Hong, Y.; Honda, R.J.; Myung, N.V.; Walker, S.L. Transport of Iron-Based Nanoparticles: Role of Magnetic Properties. *Environ. Sci. Technol.* **2009**, *43*, 8834–8839. [CrossRef] [PubMed]
7. Colombo, C.; di Iorio, E.; Liu, Q.; Jiang, Z.; Barron, V. Iron Oxide Nanoparticles in Soils: Environmental and Agronomic Importance (vol 17, pg 4449, 2017). *J. Nanosci. Nanotechnol.* **2018**, *18*, 761. [CrossRef] [PubMed]
8. Tang, W.-W.; Zeng, G.-M.; Gong, J.-L.; Liang, J.; Xu, P.; Zhang, C.; Huang, B.-B. Impact of humic/fulvic acid on the removal of heavy metals from aqueous solutions using nanomaterials: A review. *Sci. Total Environ.* **2014**, *468*, 1014–1027. [CrossRef]
9. Yang, X.; Flynn, R.; von der Kammer, F.; Hofmann, T. Quantifying the influence of humic acid adsorption on colloidal microsphere deposition onto iron-oxide-coated sand. *Environ. Pollut.* **2010**, *158*, 3498–3506. [CrossRef]
10. Akbour, R.A.; Amal, H.; Ait-Addi, A.; Douch, J.; Jada, A.; Hamdani, M. Transport and retention of humic acid through natural quartz sand: Influence of the ionic strength and the nature of divalent cation. *Colloids Surf. A-Physicochem. Eng. Asp.* **2013**, *436*, 589–598. [CrossRef]
11. Schmitt, D.; Saravia, F.; Frimmel, F.H.; Schuessler, W. NOM-facilitated transport of metal ions in aquifers: Importance of complex-dissociation kinetics and colloid formation. *Water Res.* **2003**, *37*, 3541–3550. [CrossRef]
12. Yamashita, Y.; Tanaka, T.; Adachi, Y. Transport behavior and deposition kinetics of humic acid under acidic conditions in porous media. *Colloids Surf. A-Physicochem. Eng. Asp.* **2013**, *417*, 230–235. [CrossRef]
13. Kostic, I.; Andelkovic, T.; Nikolic, R.; Bojic, A.; Purenovic, M.; Blagojevic, S.; Andelkovic, D. Copper(II) and lead(II) complexation by humic acid and humic-like ligands. *J. Serb. Chem. Soc.* **2011**, *76*, 1325–1336. [CrossRef]
14. Datta, A.; Sanyal, S.K.; Saha, S. A study on natural and synthetic humic acids and their complexing ability towards cadmium. *Plant Soil* **2001**, *235*, 115–125. [CrossRef]
15. Boguta, P.; D'Orazio, V.; Senesi, N.; Sokolowska, Z.; Szewczuk-Karpisz, K. Insight into the interaction mechanism of iron ions with soil humic acids. The effect of the pH and chemical properties of humic acids. *J. Environ. Manag.* **2019**, *245*, 367–374. [CrossRef]
16. Han, N.Z.; Thompson, M.L. Impact of dissolved organic matter on copper mobility in aquifer material. *J. Environ. Qual.* **2003**, *32*, 1829–1836. [CrossRef]
17. Han, N.; Thompson, M.L. Copper-binding ability of dissolved organic matter derived from anaerobically digested biosolids. *J. Environ. Qual.* **1999**, *28*, 939–944. [CrossRef]
18. Cheng, D.; Liao, P.; Yuan, S. Effects of ionic strength and cationic type on humic acid facilitated transport of tetracycline in porous media. *Chem. Eng. J.* **2016**, *284*, 389–394. [CrossRef]
19. Guardado, I.; Urrutia, O.; Garcia-Mina, J.M. Size distribution, complexing capacity, and stability of phosphate-metal-humic complexes. *J. Agric. Food Chem.* **2007**, *55*, 408–413. [CrossRef]
20. Liu, L.; Gao, B.; Wu, L.; Morales, V.L.; Yang, L.; Zhou, Z.; Wang, H. Deposition and transport of graphene oxide in saturated and unsaturated porous media. *Chem. Eng. J.* **2013**, *229*, 444–449. [CrossRef]
21. Corapcioglu, M.Y.; Jiang, S.Y.; Kim, S.H. Transport of dissolving colloidal particles in porous media. *Water Resour. Res.* **1999**, *35*, 3561–3565. [CrossRef]
22. Cai, L.; Tong, M.; Wang, X.; Kim, H. Influence of Clay Particles on the Transport and Retention of Titanium Dioxide Nanoparticles in Quartz Sand. *Environ. Sci. Technol.* **2014**, *48*, 7323–7332. [CrossRef] [PubMed]
23. Sen, T.K.; Khilar, K.C. Review on subsurface colloids and colloid-associated contaminant transport in saturated porous media. *Adv. Colloid Interface Sci.* **2006**, *119*, 71–96. [CrossRef]
24. Park, C.M.; Chu, K.H.; Heo, J.; Her, N.; Jang, M.; Son, A.; Yoon, Y. Environmental behavior of engineered nanomaterials in porous media: A review. *J. Hazard. Mater.* **2016**, *309*, 133–150. [CrossRef]
25. Bradford, S.A.; Torkzaban, S. Colloid transport and retention in unsaturated porous media: A review of interface-, collector-, and pore-scale processes and models. *Vadose Zone J.* **2008**, *7*, 667–681. [CrossRef]
26. Torkzaban, S.; Bradford, S.A.; van Genuchten, M.T.; Walker, S.L. Colloid transport in unsaturated porous media: The role of water content and ionic strength on particle straining. *J. Contam. Hydrol.* **2008**, *96*, 113–127. [CrossRef]
27. Massoudieh, A.; Ginn, T.R. Modeling colloid-facilitated transport of multi-species contaminants in unsaturated porous media. *J. Contam. Hydrol.* **2007**, *92*, 162–183. [CrossRef]
28. Shen, Q.; Xia, K.; Zhang, S.; Kong, C.; Hu, Q.; Yang, S. Hyperspectral indirect inversion of heavy-metal copper in reclaimed soil of iron ore area. *Spectrochim. Acta Part A-Mol. Biomol. Spectrosc.* **2019**, *222*. [CrossRef]

29. Almeida, V.O.d.; Pereira, T.C.B.; Teodoro, L.d.S.; Escobar, M.; Ordovas, C.J.; Dos Santos, K.B.; Weiler, J.; Bogo, M.R.; Schneider, I.A.H. On the effects of iron ore tailings micro/nanoparticles in embryonic and larval zebrafish (Danio rerio). *Sci. Total Environ.* **2020**, 143456. [CrossRef]
30. Rybnikova, V.; Usman, M.; Hanna, K. Removal of PCBs in contaminated soils by means of chemical reduction and advanced oxidation processes. *Environ. Sci. Pollut. Res.* **2016**, *23*, 17035–17048. [CrossRef]
31. Chen, M.; Tao, X.; Wang, D.; Xu, Z.; Xu, X.; Hu, X.; Xu, N.; Cao, X. Facilitated transport of cadmium by biochar-Fe3O4 nanocomposites in water-saturated natural soils. *Sci. Total Environ.* **2019**, *684*, 265–275. [CrossRef] [PubMed]
32. Fan, W.; Jiang, X.; Lu, Y.; Huo, M.; Lin, S.; Geng, Z. Effects of surfactants on graphene oxide nanoparticles transport in saturated porous media. *J. Environ. Sci.* **2015**, *35*, 12–19. [CrossRef]
33. Fan, W.; Jiang, X.H.; Yang, W.; Geng, Z.; Huo, M.X.; Liu, Z.M.; Zhou, H. Transport of graphene oxide in saturated porous media: Effect of cation composition in mixed Na-Ca electrolyte systems. *Sci. Total Environ.* **2015**, *511*, 509–515. [CrossRef]
34. Zhou, D.D.; Jiang, X.H.; Lu, Y.; Fan, W.; Huo, M.X.; Crittenden, J.C. Cotransport of graphene oxide and Cu(II) through saturated porous media. *Sci. Total Environ.* **2016**, *550*, 717–726. [CrossRef] [PubMed]
35. Ghosh, S.; Jiang, W.; McClements, D.J.; Xing, B. Colloidal Stability of Magnetic Iron Oxide Nanoparticles: Influence of Natural Organic Matter and Synthetic Polyelectrolytes. *Langmuir* **2011**, *27*, 8036–8043. [CrossRef] [PubMed]
36. Bayat, A.E.; Junin, R.; Derahman, M.N.; Samad, A.A. TiO2 nanoparticle transport and retention through saturated limestone porous media under various ionic strength conditions. *Chemosphere* **2015**, *134*, 7–15. [CrossRef] [PubMed]
37. Yang, Y.; Zhang, Y. Hysteresis and kinetic characteristics of Copper sorption and desorption on old manured loessal soil. *Chin. J. Soil Sci.* **2000**, 248–250+285.
38. Chen, L.; Zhu, Y.-Y.; Luo, H.-Q.; Yang, J.-Y. Characteristic of adsorption, desorption, and co-transport of vanadium on humic acid colloid. *Ecotoxicol. Environ. Saf.* **2020**, *190*. [CrossRef]
39. Yang, Y.; Hu, M.; Zhou, D.; Fan, W.; Wang, X.; Huo, M. Bioremoval of Cu2+ from CMP wastewater by a novel copper-resistant bacterium Cupriavidus gilardii CR3: Characteristics and mechanisms. *RSC Adv.* **2017**, *7*, 18793–18802. [CrossRef]
40. Brigante, M.; Schulz, P.C. Remotion of the antibiotic tetracycline by titania and titania-silica composed materials. *J. Hazard. Mater.* **2011**, *192*, 1597–1608. [CrossRef]
41. Giovanela, M.; Crespo, J.S.; Antunes, M.; Adamatti, D.S.; Fernandes, A.N.; Barison, A.; da Silva, C.W.P.; Guegan, R.; Motelica-Heino, M.; Sierra, M.M.D. Chemical and spectroscopic characterization of humic acids extracted from the bottom sediments of a Brazilian subtropical microbasin. *J. Mol. Struct.* **2010**, *981*, 111–119. [CrossRef]
42. Fan, W.; Guo, T.; Gao, S.; Lu, Y.; Meng, Y.; Huo, M. Evolution of dissolved organic matter during artificial groundwater recharge with effluent from underutilized WWTP and the resulting facilitated transport effect. *Environ. Res.* **2020**, *193*, 110527. [CrossRef] [PubMed]
43. Lu, Z.H.; Prouty, M.D.; Guo, Z.H.; Golub, V.O.; Kumar, C.; Lvov, Y.M. Magnetic switch of permeability for polyelectrolyte microcapsules embedded with Co@Au nanoparticles. *Langmuir* **2005**, *21*, 2042–2050. [CrossRef] [PubMed]
44. Peng, L.; Qin, P.; Lei, M.; Zeng, Q.; Song, H.; Yang, J.; Shao, J.; Liao, B.; Gu, J. Modifying Fe3O4 nanoparticles with humic acid for removal of Rhodamine B in water. *J. Hazard. Mater.* **2012**, *209*, 193–198. [CrossRef]
45. Zhao, T.; Fang, M.; Tang, Z.; Zhao, X.; Xie, F.; Wu, F.; Giesy, J.P. Effects of fulvic acid on aggregation, sedimentation, and adsorption of Fe3O4 magnetic nanoparticles. *Environ. Sci. Pollut. Res.* **2019**, *26*, 21463–21474. [CrossRef]
46. Liu, X.Q.; Ma, Z.Y.; Xing, J.M.; Liu, H.Z. Preparation and characterization of amino-silane modified superparamagnetic silica nanospheres. *J. Magn. Magn. Mater.* **2004**, *270*, 1–6. [CrossRef]
47. Barancikova, G.; Makovnikova, J. The influence of humic acid quality on the sorption and mobility of heavy metals. *Plant Soil Environ.* **2003**, *49*, 565–571. [CrossRef]
48. Kalina, M.; Klucakova, M.; Sedlacek, P. Utilization of fractional extraction for characterization of the interactions between humic acids and metals. *Geoderma* **2013**, *207*, 92–98. [CrossRef]
49. Fang, J.; Xu, M.-J.; Wang, D.-J.; Wen, B.; Han, J.-Y. Modeling the transport of TiO2 nanoparticle aggregates in saturated and unsaturated granular media: Effects of ionic strength and pH. *Water Res.* **2013**, *47*, 1399–1408. [CrossRef]
50. Lenhart, J.J.; Saiers, J.E. Transport of silica colloids through unsaturated porous media: Experimental results and model comparisons. *Environ. Sci. Technol.* **2002**, *36*, 769–777. [CrossRef]
51. Won, J.; Burns, S.E. Role of Immobile Kaolinite Colloids in the Transport of Heavy Metals. *Environ. Sci. Technol.* **2018**, *52*, 2735–2741. [CrossRef] [PubMed]
52. Reddad, Z.; Gerente, C.; Andres, Y.; Le Cloirec, P. Adsorption of several metal ions onto a low-cost biosorbent: Kinetic and equilibrium studies. *Environ. Sci. Technol.* **2002**, *36*, 2067–2073. [CrossRef] [PubMed]
53. Pan, D.-Q.; Fan, Q.-H.; Li, P.; Liu, S.-P.; Wu, W.-S. Sorption of Th(IV) on Na-bentonite: Effects of pH, ionic strength, humic substances and temperature. *Chem. Eng. J.* **2011**, *172*, 898–905. [CrossRef]
54. Wu, X.L.; Zhao, D.; Yang, S.T. Impact of solution chemistry conditions on the sorption behavior of Cu(II) on Lin'an montmorillonite. *Desalination* **2011**, *269*, 84–91. [CrossRef]
55. Xiao, J.; Zhao, L.; Zhang, W.; Liu, X.; Chen, Y. Effect of pH, ionic strength, foreign ions, humic acid and temperature on Zn(II) sorption onto gamma-Al2O3. *Korean J. Chem. Eng.* **2014**, *31*, 253–261. [CrossRef]